PAPER • OPEN ACCESS

Polymer powder bed fusion surface texture measurement

View the article online for updates and enhancements.

Polymer powder bed fusion surface texture measurement

Marc-Antoine de Pastre[1,2]**, Adam Thompson**[1] ⓘ**, Yann Quinsat**[2] ⓘ**,
José A Albajez García**[3]**, Nicola Senin**[1,4] ⓘ **and Richard Leach**[1]

[1] Manufacturing Metrology Team, Faculty of Engineering, University of Nottingham, Nottingham, United Kingdom
[2] ENS Paris-Saclay, Université Paris-Saclay, Cachan, France
[3] Manufacturing Engineering and Advanced Metology Group, I3A, University of Zaragoza, Zaragoza, Spain
[4] Department of Engineering, University of Perugia, Perugia, Italy

E-mail: adam.thompson@nottingham.ac.uk

CrossMark

Abstract

Polymer laser powder bed fusion (LPBF) surfaces can be challenging to measure. These surfaces comprise complex features including undercuts, deep recesses, step-like transitions, a large range of measurement scales and unfavourable optically materials properties. While recent research has begun to examine the nature of these surfaces, there has not yet been significant effort in understanding how different measurement instruments interact with them. In this paper, we compare the results of LPBF surface topography measurements using a series of different instrument technologies, including contact stylus, focus variation microscopy, coherence scanning interferometry, laser scanning confocal microscopy and x-ray computed tomography. Measurements are made on both side and top surfaces of a cubic polyamide-12 LPBF sample. Different instrument behaviours are highlighted through qualitative visual inspection of surface reconstructions. Further comparisons are then performed through evaluation of profile and areal surface texture parameters and statistical modelling of surface topographies. These analyses allow for the identification both of discrepancies between texture parameters and discrepancies between local topographies reconstructed from measurements. Instrument repeatability metrics are also presented for each measurement of the test surfaces. Results show that discrepancies in measurements made on the acquired datasets are often similar in magnitude to the size of the features present on the surfaces. Conclusions are drawn regarding the suitability of various surface measurement instruments for polymer LPBF surfaces.

Keywords: additive manufacturing, polymer powder bed fusion, surface metrology, data comparison

(Some figures may appear in colour only in the online journal)

1. Introduction

Additive manufacturing (AM) is now fully capable of producing functional parts for a variety of high-value applications [1, 2], allowing for the creation of geometries that are not possible using conventional subtractive or formative manufacturing methods [1]. Examples of these geometries include lattices and other complex structures that often contain features inaccessible to conventional machine tools [3].

The most developed of the AM technologies fall into the powder bed fusion process family [4]. Laser powder bed fusion (LPBF) is of particular interest to the manufacturing community, because it does not require support structures when using polymer materials. Not needing support structures means that there is a significant design freedom afforded to parts made using polymer LPBF, even when compared to

other AM technologies [5]. LPBF involves the selective fusion of thin layers of powder by a scanning laser, successively spread by a roller within a building chamber [1, 5, 6].

The precision and accuracy of LPBF systems remains poor in comparison to established methods (e.g. subtractive manufacturing), and its capability for meeting demanding design tolerances remains at an often unacceptable level for many manufacturers, so finishing operations are required [3]. LPBF parts, and indeed, AM parts in general, have suffered until recently from a lack of understanding of the physics of the underlying processes. Research is underway in process simulation to better understand the physical interactions taking place in the system during fabrication [7–9], and also in post-process investigation of parts produced by LPBF. Such after-the-fact investigation allows a manufacturer to characterise a process, and to better understand the 'fingerprint' left behind by it [10]. For example, measurement and characterisation of surface topography can allow a manufacturer to reconstruct how that topography was formed, leading to an improved understanding of the process that created it (as shown by Senin *et al* [10]).

For surface characterisation to be of benefit, research is required to understand the surfaces produced by a manufacturing process, the features present on these surfaces, and how these features relate to physical phenomena occurring during the process. Surfaces should be studied in depth, and a co-creation process should ideally take place between the manufacturer and the metrologist, to develop measurement and characterisation pipelines that facilitate the development of improved process understanding [10]. In the co-creation model, a concerted effort should be made by researchers in manufacturing and metrology, to identify the relevant topographic features that should be isolated for analysis, and how they should be described in terms of their geometric properties. The requirement for this identification process is particularly highlighted in the review of methods for characterising metal AM surface texture by Townsend *et al* [11].

Feature-based investigations of topography have recently been conducted for metal LPBF parts, involving the identification and characterisation of signature topographic formations present on surfaces [11–13]. For example, Senin *et al* [10, 14] compared non-contact methods of surface topography data acquisition, observing how different measurement technologies led to different topographic reconstructions of metal LPBF surfaces. The authors examined measured topography data using qualitative visual assessment, ISO 25178-2 surface texture parameters [15, 16], direct comparison using statistical modelling of topographies and feature-based analysis methods. The primary conclusion was that the measured shape of a feature is intimately linked to the type of instrument used, its setup and the measuring conditions. Discrepancies between instruments were observed on the same order of magnitude as the size of the features being measured.

While a significant bulk of work has been performed in the investigation of metal LPBF surfaces, polymer LPBF surfaces have not been studied to the same depth. Thus far, most of the work performed on polymer LPBF parts has been in studying the effect of altering printing parameters on ISO 4287 texture

parameters [17, 18], without delving deeper into features present on such surfaces and how these features relate to the process itself. Most notably, laser power and scan speed are noted as the most significant adjustable parameters that influence surface texture [19, 20].

There has been limited research on comparing measurement methods for polymer LPBF surfaces. An approach for surface texture evaluation on a polyamide-12 sintered cube with different methods was recently proposed by Vetterli *et al* [21]. In this work, the cube top, bottom and side surfaces were examined, with Vetterli *et al* presenting *Ra* and *Rz* ISO 4287 parameters [17] for each surface, measured in two orthogonal directions and each measured with two different contact stylus instruments. Contact measurements were compared to confocal and interferometric measurements, optical micrographs and cross-sectional profiles extracted from areal data acquired using an optical technique that obtains data using a reflective skin spread on an elastomer sensor [22]. Considering the time required to measure, Vetterli *et al* argue that although contact stylus instruments seem to capture texture information in the shortest time period, optical methods provide a better information-to-time ratio than contact stylus instruments. Contact and non-contact methods are also compared by Launhardt *et al* [23], where measurements are made and *Ra*, *Rz*, *Sa* and *Sz* parameters are generated for a polyamide-12 tensile bar fabricated using AM. Two different contact stylus systems were compared for their performance in profile acquisition, while areal data were acquired for comparison using focus variation, fringe projection and confocal laser scanning microscopy. Similar trends were observed between different instruments for the computed *Ra* and *Sa* values. Launhardt *et al* also identified that contact stylus measurements are liable to damage polymer surfaces, inducing potentially significant effects on the surface topography. Moreover, because of the low reflectivity of the material, Launhardt *et al* noted that polymer LPBF surfaces are challenging to measure using optical methods.

In this paper, using methods presented previously [9, 14], we begin the process of deepening the understanding of polymer LPBF surfaces by examining how different optical areal measurement instruments reconstruct the topography of polymer LPBF surfaces We use multiple measurements acquired from the same area to provide qualitative and quantitative analysis of surface reconstructions, using ISO 25178-2 parameters as well as direct topography comparison using the statistical topography comparison method outlined in [14]. Further, we provide a comparison of data acquired using optical systems to data acquired using a contact system, by extracting profiles from areal optical data.

2. Methodology

2.1. Measurement technologies

We considered three of the most common areal surface measurement technologies: laser scanning confocal microscopy (CM) [24,25], focus variation (FV) [26, 27] and coherence scanning interferometry (CSI) [28–31]. Additionally, we
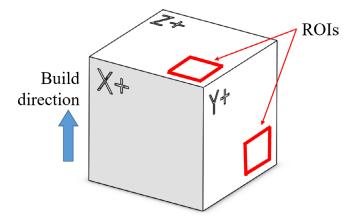
Figure 1. The studied sample.

measured the test surfaces using x-ray computed tomography (XCT) and a contact stylus profile measurement system. XCT has recently been demonstrated capable of providing surface measurement results that are comparable to results provided by established optical measurement systems [32, 33]. Stylus measurement is the most common method of surface data acquisition, despite only capturing profile (as opposed to areal) data [11] unless equipped with a lateral stage. Comparisons were then performed between data acquired using each of these methods, measuring the same area of the test surfaces using each instrument. For this purpose, reconstructed surface topographies were aligned in a single co-ordinate system and similarly cropped using the dedicated relocation algorithm discussed in previous work (see [9, 14] and section 2.3.2).

2.2. Examined sample

The sample used was a polyamide-12 cube of size $(20 \times 20 \times 20)$ mm, produced using an EOS FORMIGA P110 with the following setup, in line with the machine manufacturers' guidance for processing this material: layer thickness of 100 µm, hatch scan power of 21 W, contour scan power of 16 W, scan speed of 2500 mm s^{-1}, hatch spacing of 250 µm and build volume temperature of 172° (see figure 1). The part was cleaned following production, using the three-step process commonly employed to clean parts fabricated using polymer LPBF: the part was blasted with compressed air, washed with water and finally dried in an oven. Two regions of interest (ROIs) were selected on the sample, representative of 'side' and 'top' surfaces with respect to the build direction, shown in previous work to be significantly different from one another [21] (see the red squares in figure 1). Surfaces built at other angles or using different machine settings could have been included in this work, but side and top surfaces were assumed to be broadly representative of the range of polymer LPBF surfaces for simplicity.

2.3. Measurement setups and data processing

2.3.1. Data acquisition.

2.3.1.1. Areal data. In each case, a corner of the cube was included in the measured area and used to relocate topography

data acquired using different measurement systems. The ROIs were subsequently cropped from within the total measured area, to remove effects present near the edges and corners of the cube. Because of differences between the instruments/setups, the total measured areas varied slightly between systems, but were all approximately (3×3) mm in size. The cropped ROIs were (2.5×2.5) mm in size. This size was chosen in contrast to the (8×8) mm area suggested as the default in ISO 25178-3 [34] because of data size limitations imposed by the current implementation of the analysis process. To measure using sufficiently high resolution to resolve the smallest features present on these surfaces, the wider (8×8) mm area becomes too large to process because of the computational expense of such large datasets. However, recent work examining the measurement of metal LPBF surfaces [9, 14, 35] has shown that an area of (2.5×2.5) mm is of sufficient size to evaluate such surfaces.

Commercial instruments were used to perform CSI, FV and XCT measurements, while CM measurements were made using a research instrument. All instrument names have been redacted to prevent direct comparison of commercial instruments. In the descriptions below, FoV is the field of view, LR is the lateral resolution and NA is the numerical aperture. In each case, LR-pixel refers to the pixel spacing of the detector used by each instrument, LR-optical refers the calculated Sparrow optical limit of each instrument and LR-contrast refers specifically to a reference radius defining the width of the local window used by the FV measurement technology to compute local contrast (needed to compute local height at the measured location). The Sparrow limit was calculated using a wavelength of 580 nm for the broadband systems (CSI and FV) and 520 nm for the laser CM system. The following measurement setups were used for both side and top areal topography measurements.

- CM: 5× objective lens (NA 0.13, FoV (1.16×0.95) mm, LR-pixel (x axis) 2.27 µm LR-pixel (y axis) 1.85 µm, LR-optical 0.63 µm), measured area (3.24×2.97) mm, stitching of multiple individually acquired FoVs performed in MountainsMap [36].
- CSI: 5.5× objective lens at $1 \times$ zoom, (NA 0.15, FoV (1.56×1.56) mm, LR-pixel 1.571 µm, LR-optical 1.82 µm), measured area (4.2×4.2) mm, stitching of multiple FoVs performed in the manufacturer software.
- FV: 10× objective lens, (NA 0.3, FoV (1.62×1.62) mm LR-pixel, 0.88 µm, LR-optical 0.91 µm, LR-contrast 2.77 µm), coaxial illumination, measured area (4.5×4.5) mm, stitching of multiple FoVs performed in the manufacturer's software.
- XCT: geometric magnification of 20×, leading to a voxel size of 10 µm. Volumetric reconstruction was performed from 3142 X-ray projections (each formed from averaging of two exposure per projection, each lasting 2 s), tube voltage 105 kV, tube current 95 µA, 0.1 mm copper pre-filter. A warmup scan of approximately one hour was performed prior to the scans and data were reconstructed in the manufacturer software, using no beam hardening correction and a ramp filter. Surfaces (triangulated
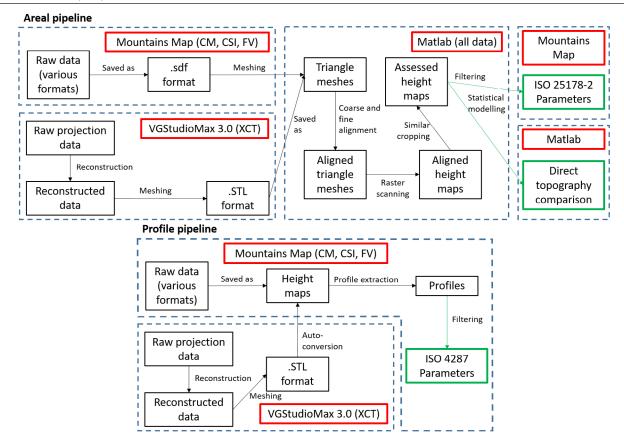
Areal pipeline

Figure 2. Data processing pipelines for profile and areal cases.

meshes) were determined in VGStudio MAX 3.0 [37] from volumetric data, using the maximum gradient method over four voxels, with the ISO-50 isosurface as a starting point [38]. Determined surfaces were outputted as triangle meshes in STL format.

In each measurement setup, the sample was measured five times consecutively without moving the part between measurements for both side and top surfaces.

2.3.1.2. Profile data. A comparison was made between the optical instruments and a contact stylus instrument, to provide a check on the performance of the optical systems by relying upon the well-understood physics of a contact based measurement system [39]. An area similar to the ROI discussed in section 2.2 was measured using the same measurement setups as outlined above, with modified measured area dimensions to account for the need for profile evaluation lengths of 4 mm (in each case, one FoV × 5 mm) [35]. Tactile measurements were made using a contact stylus instrument with a 2 μm tip radius. Stylus measurements were made after all optical measurements were completed, to prevent any modification of the surface from the contact-based measurement process.

2.3.2. Data extraction and comparison.
2.3.2.1. Areal data. Raw data (height maps) from CM, CSI and FV systems were converted into a standard format (.SDF), using the software MountainsMap. The height maps were then imported into Matlab [40]. XCT surface data, available as STL

models, were also imported into Matlab [33, 41]. Height maps were converted into triangle meshes by virtual raster scanning [9, 14] and co-localised by rigid transformations (rotation, translation) within a single co-ordinate system. Co-localisation was performed in two stages, involving an initial coarse localisation based on alignment of visually recognisable landmarks [42], followed by an automated fine alignment using an iterative closest point algorithm [43] as per the method described in [9, 14]. To co-localise the data, a single CSI dataset was arbitrarily chosen as the 'master' dataset, and one dataset from each instrument was chosen as a 'sub-master'. The FV, XCT and CM sub-masters were aligned to the master CSI dataset, and all remaining datasets were aligned to their respective sub-master. This method maximises the quality of the alignment within a set of repeats from one instrument. We assume for this study that discrepancies between datasets resulting from poor alignment are negligible compared to the discrepancies between measured datasets (see [14]). Following co-localisation, the triangle meshes were converted into height maps at a resolution approximately equivalent to that of the dataset with the lowest lateral resolution (5 μm) using the method described in [9, 14]. This resolution is approximate as the lateral resolution of XCT surface topography measurement is poorly defined [38], but 5 μm was chosen as equivalent to half of the voxel size. Finally, all the aligned height maps were similarly cropped and (2.5 × 2.5) mm ROIs were extracted. The areal data processing pipeline is shown in the upper portion of figure 2.
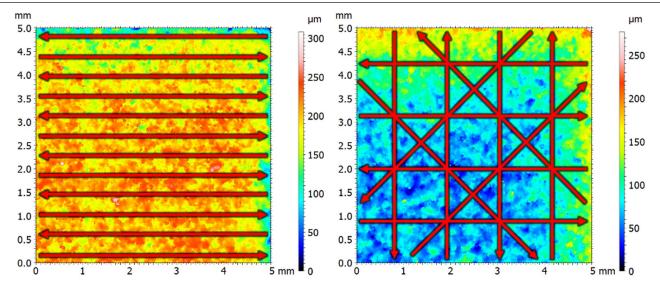
Figure 3. Illustration of the contact stylus measurement pattern for the side (left) and top surfaces (right), overlaid on example levelled, unfiltered FV datasets.

2.3.2.2.Profile data. Raw data from CM, CSI and FV systems were imported into MountainsMap as height maps, while raw data from the contact stylus system were imported as profiles. XCT data were imported into MountainsMap and automatically converted into height maps at a spatial resolution automatically determined by MountainsMap to match the point density of the original triangulated mesh ((4.80×5.34) μm for the top surface and (3.77×5.49) μm for the side surface). Profiles were then extracted from areal data in MountainsMap from single measurements made with each optical measurement system of the same approximate area, measured using the same measurement setups described above. In all cases, profiles were acquired as per the patterns shown in figure 3. For side surfaces, 12 equally-spaced 5 mm long profiles were acquired by scanning perpendicular to the main visible lay (i.e. the layer structure), while 12 linear, 5 mm paths were defined on the top surface in various directions, to account for the lack of a discernible lay on this surface. The areal data processing pipeline is shown in the lower portion of figure 2.

2.4. Comparison methods

2.4.1. Qualitative comparisons. Visual inspection was performed in MountainsMap on 3D and 2D geometric models reconstructed, respectively, from the height maps and profiles, noting visible similarities and discrepancies. Features present on the surfaces were identified at different scales.

2.4.2. ISO parameter evaluation. Surface texture parameter evaluation is the main tool used in research and industry to describe surface topographies [9]. Commonly used parameters were generated for the measured surfaces and compared statistically. All filtering and computation of parameters was performed in MountainsMap, while statistical testing was performed in Minitab [44].

2.4.2.1.ISO 25178-2 areal surface texture parameters. From the measured surface, primary surfaces were obtained by application of an S-filter with a nesting index of 5 μm, to match the resolution chosen when resampling the triangle meshes into height maps after the co-localisation process. An F-operator was then applied (least-squares mean plane removal by subtraction) to provide SF surfaces. SL surfaces were also generated through the use of an L-filter with a nesting index of 0.8 mm. The index of 0.8 mm was chosen based upon values used in the existing literature [14]. Four of the most commonly used ISO 25178-2 [15, 16] surface texture parameters, *Sa*, *Sq*, *Ssk* and *Sku*, were then generated and compared for each of the forty acquired surface datasets in the SF and SL cases. Confidence intervals (CIs) of the mean at 95% confidence were estimated for each parameter using *t*-distributions generated for both surfaces using five repeat measurements acquired using each of the four instruments. *T*-distributions are used instead of Gaussian distributions throughout this work because of the small sample sizes examined.

2.4.2.2.ISO 4287 profile surface texture parameters. From the measured profiles, primary profiles were obtained by application of a λ_s filter with a cut-off set at 2.5 μm. A form removal operation was then applied using least-squares mean line removal by subtraction and a λ_c filter with a cut-off set at 0.8 mm was applied. Profile ends were removed to provide an evaluation length of 4 mm. ISO 4287 [17] *Ra* and *Rq* parameters were computed for each of the 120 acquired profiles and CIs of the means at 95% confidence were estimated for each parameter using *t*-distributions. *t*-distributions were generated for both surfaces using 12 repeat measurements acquired using each of the five instruments. *Ra* and *Rq* were chosen as the two most common profile parameters to provide a simple comparison between optical and contact methods.

It should be noted that for surfaces where 10 μm < *Ra* < 80 μm (i.e. surfaces such as those examined in this work), ISO 4288 [45] recommends an evaluation length of 40 mm and λ_s and λ_c filters of 25 μm and 8 mm, respectively. However, work by Triantaphyllou *et al* [35] showed that it is possible to evaluate such surfaces using a 4 mm evaluation length and
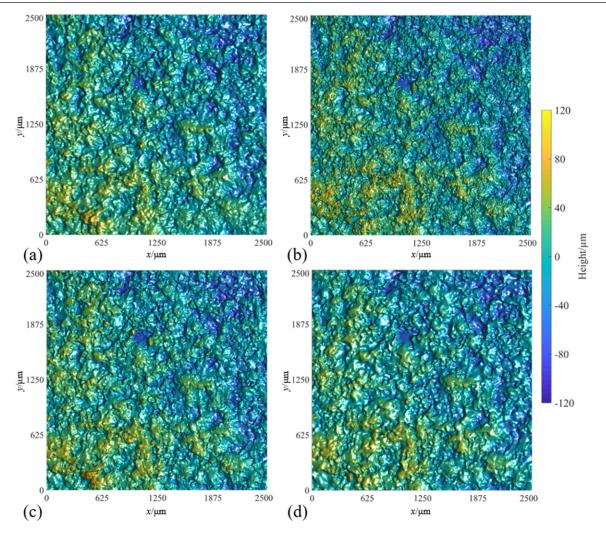
Figure 4. Example unfiltered side surface topographies: (a) CM, (b) CSI, (c) FV and (d) XCT.

λ_s and λ_c filters of 2.5 µm and 0.8 mm, respectively. It can be noted that the chosen λ_s filter (2.5 µm) is different from the chosen S-filter (5 µm) used above in the areal case. While the S-filter chosen above was selected to best match the spatial measurement bands of the instruments in the areal case, 2.5 µm was chosen in the profile case to match the filtering conditions generally used when performing stylus measurements with a 2 µm radius tip.

2.4.3. Direct topography comparison. A recently developed method for point-by-point comparison of surface topographies [14] was applied in this work. Using the five aligned datasets acquired by each measurement system, mean surfaces were computed for each instrument. For the direct topography comparisons, data are not filtered using Gaussian filters as described in section 2.4.2, but instrument spatial frequency response bands are intrinsically matched as part of the alignment process (see [9, 14, 47]). CIs for the mean surfaces were then estimated on a point-by-point basis using *t*-distributions at 95% confidence. Mean width of the CIs was calculated as a repeatability metric, and CIs were plotted on a point-by-point basis, to quantify the variation in repeatability across the surface. Global discrepancy between instrument pairs was then computed, defined as the percentage of the surface area where CIs do not overlap. It should be noted that discrepancy may also exist in overlapping areas, as this is a statistical test and so is only capable of declaring discrepancy with a specific confidence. As such, CI overlap does not necessarily mean agreement, but rather than disagreement cannot be explicitly disproven. In addition to the use of CI width as an indication of local repeatability, local bias between the examined instruments was assessed by identifying the regions where the CIs of different instruments do not overlap. If the CSI measurement is taken as the metrological reference (i.e. unbiased measurement result), then discrepancy with respect to the CSI data becomes an indication of local bias. CSI was chosen as the reference as CSI data are typically associated with the lowest mean width of the CIs in both the side and top surface cases. Local bias between instrument pairs (i.e. the distance between the means of the two statistical topography models) was finally plotted to visualise areas of the surface that cause greater and smaller discrepancies.
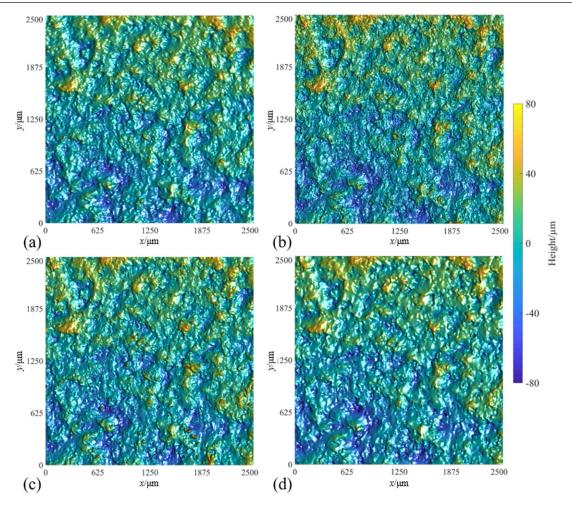
Figure 5. Example unfiltered top surface topographies: (a) CM, (b) CSI, (c) FV and (d) XCT.
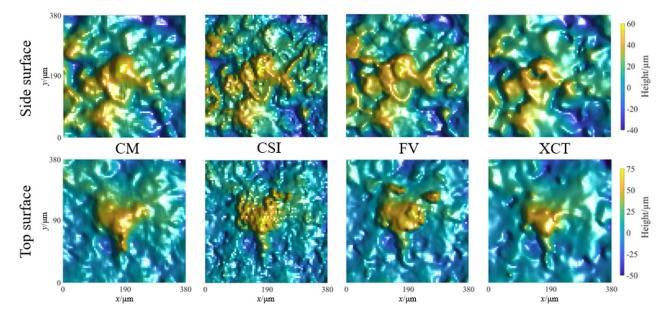

Figure 6. Instrument acquisition of an unfiltered side and a top surface feature (FoV: 0.38 mm × 0.38 mm).
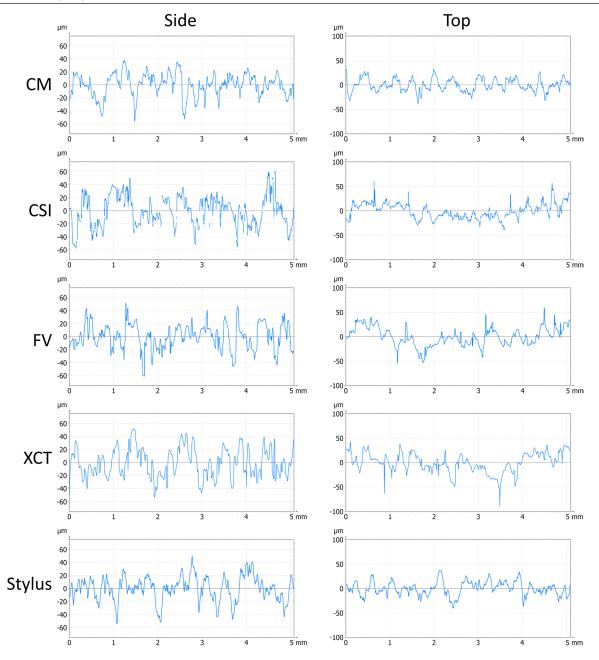
Figure 7. Example unfiltered profile topographies. Differences in *z*-axis scale should be noted between top and side surfaces.

3. Results

3.1. Qualitative comparison of aligned topographies

3.1.1. Areal data. In figures 4 and 5, qualitative overviews of the aligned height maps are provided for both side and top surfaces, respectively. Height maps are presented in these figures in their unlevelled states (i.e. before application of the *F*-operator). Both types of surface appear to be similar in terms of the topographic formations present, with formations seemingly randomly distributed in both cases. Although side surfaces present a lay that is visible to the naked eye, no discernible lay is visible in either case when visualised in the figures below. Qualitative similarity also exists between

instruments, with few obvious visible differences. Zoomed in regions of each dataset are presented in figure 6, to show how each instrument reconstructs example features on the surface.

3.1.2. Profile data. In figure 7, qualitative overviews of example profiles are provided for both side and top surfaces. These profiles are not aligned with one another so should not be identical, but are representative of the set of profiles acquired using each instrument. Profiles have been levelled for this visualisation. As in the areal case, both types of surface appear to be similar in terms of the topographic formations present, with formations seemingly randomly distributed in both cases. Qualitative similarity also exists between instruments, with few obvious visible differences.
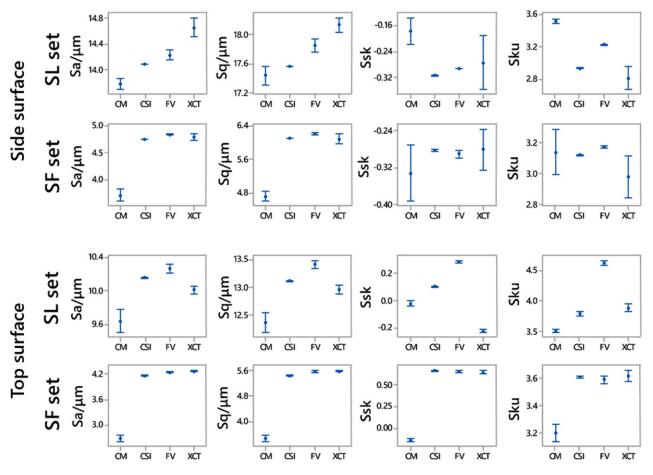
Figure 8. Filtered ISO 25178-2 [15] parameters for side and top surfaces.

3.2. Texture parameter comparison

3.2.1. Areal data. For both the SF and SL cases, ISO 25178-2 [15] *Sa*, *Sq*, *Ssk* and *Sku* surface texture parameters with confidence intervals on the mean at 95% confidence are plotted for each surface in figure 8. Statistical discrepancy is seen between instruments for all parameters, though cases where discrepancy cannot be demonstrated (i.e. overlapping CIs) also exists in many cases. When compared to the other examined instruments, CM returned statistically different parameter values most often and by the largest amount. The CI widths (i.e. repeatability) are similar between each instrument, with CSI consistently returning the smallest CIs. FV was the next-most repeatable, while CM was consistently the least repeatable instrument for texture parameters. The areal field texture parameters *Ssk* and *Sku* were found generally less repeatable than *Sa* and *Sq*, particularly when obtained from CM and XCT data. These observations are different from previous work on metal LPBF [14].

3.2.2. Profile data. ISO 4287 [17] *Ra* and *Rq* texture parameters with confidence intervals on the mean, computed at 95% confidence, are plotted for each surface in figure 9. Statistical disagreement between optical and contact measurements is seen in the side surface case, and in the top surface case when compared to the FV and XCT

results. In all cases, the mean parameter values returned by the contact stylus system are lower than those reported for the optical systems.

3.3. Direct topography comparison

The mean width of the local CIs associated to the statistical topography models are presented for each surface and each instrument in figure 10. These widths are consistently higher for the side surface than for the top surface. For CM, CSI and FV, the ratio of the side CI width to the top CI width is similar (1.2 to 1.4). This ratio is not the same for the XCT data, however, where the ratio is 3.3. The point-by-point CIs for each surface are presented in figure 11, highlighting regions of the surface where repeatability is poor and where repeatability is good. Overall discrepancies between instrument pairs are presented in table 1.

Global discrepancy between mean surfaces is presented in figure 12, while local bias between mean surfaces is presented in figure 13. The mean unsigned bias between instruments is consistently below 2 μm, but varies substantially between 0.5 μm and 1.75 μm with no discernible trend. Local bias between the examined instrument maps show concentrated increases in bias surrounding specific features, and a bow in the data is visible in the in the CM/CSI top surface case.
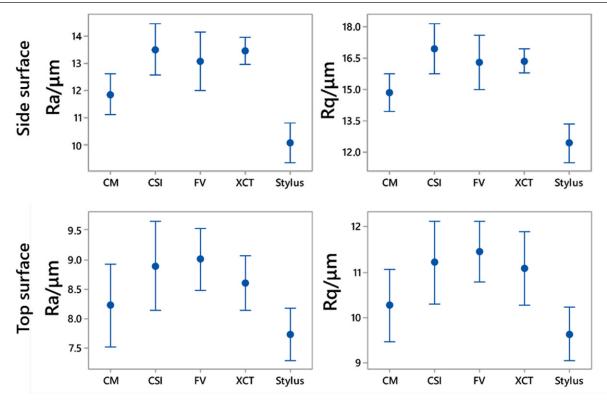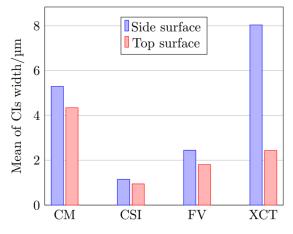
Figure 9. Filtered ISO 4287 [17] parameters for side and top surfaces.

Figure 10. Mean CI widths for the examined spatial frequency band matched surfaces.

4. Discussion

Side and top surfaces (figures 4, 5 and 7) provide similar results in terms of qualitative, visual assessment. In both cases, there are no obviously identifiable features akin to those commonly found on metal powder bed fusion surfaces [9], and the features present appear (at least visually) to be randomly distributed. Representation of both surfaces by the various instruments is broadly similar, with some differences visible when examining smaller scale features (figure 6) on both surfaces. It is not clear from the data what the cause of these discrepancies is, but likely options include complex optical effects that result from measurement of translucent surfaces, where sub-surface reflections distort each instruments' response to the surface (e.g. see [27]). Further research is required in optimisation of

each measurement technology, to understand the exact cause of these discrepancies.

The values taken by ISO 4287 [17] and 25178-2 [15] parameters (as shown in figures 8 and 9) show that side surfaces are slightly rougher than top surfaces (with higher Ra, Rq, Sa and Sq parameters as measured by all instruments). The areal skewness of side surfaces was negative, while for top surfaces it was positive. Kurtosis values were slightly higher in the top surface case than the side surface case. While often statistically discrepant, CIs on parameter mean values were small in comparison to the values of the parameters themselves, and parameters took quantitatively similar values for all instruments. Contact stylus measurement returned notably lower parameter values than the non-contact optical systems. These lower values may be due to the aforementioned optical effects when measuring translucent samples, the contact nature of the measurement process or the location of the specific profiles extracted or some other local or widespread effects. Additionally, while the probing force is low, the relatively soft polyamide-12 being measured may have been scratched by the stylus during measurement, removing the tops of peaks. As the recorded profiles are likely to be of the scratched surface as opposed to the raw surface, this scratching may have had the effect of reducing the measured Ra and Rq values with respect to the non-contact methods. While no discernible scratches were visible during subsequent qualitative microscopic evaluation, such peak removal may be impossible to detect in areal visualisations of measurements. In any case, the specific reason cannot be discerned from the data and further work is required to make conclusions about the existence of reduced parameter values in the contact case.
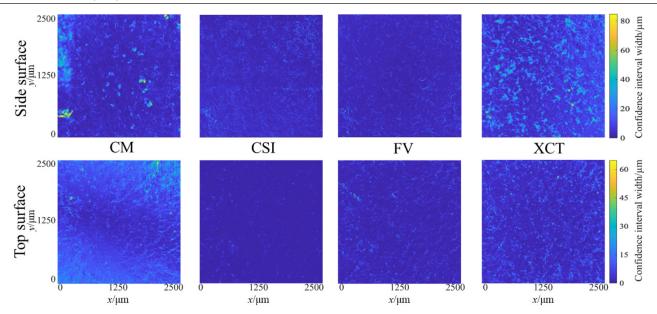
Figure 11. Point-by-point CIs for each spatial frequency band matched measurement setup.

Table 1. Discrepancies between instrument pairs.

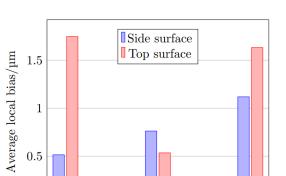| Instrument pair	CSI/ FV	CSI/ XCT	CSI/ CM	FV/ XCT	FV/ CM	XCT/ CM
Side surface discrepancy/%	41.51	38.64	45.15	27.11	35.87	24.37
Top surface discrepancy/%	58.25	45.87	39.23	54.06	39.78	32.74

Figure 12. Global discrepancy between instrument pairs, comparing each measurement to CSI.

Regardless, while they are in some cases statistically discrepant, the parameters generated using each measurement method are similar in magnitude for both contact and non-contact methods, implying that measurement of these surfaces is possible using all of the examined instruments.

A note should be made about comparing surface texture parameter CI overlap as a method for assessing instrument performance. When CIs do not overlap, it is safe to say that results are different (i.e. the difference is statistically significant). When CIs do overlap, the conventional interpretation should be that there is not enough evidence to state that the results are different. In truth, the difference may still be

statistically significant even when CIs do overlap, but the test is not powerful enough to detect it. A similar issue would be encountered by applying ANOVA as an alternative method of investigation. In such an analysis, significant inhomogeneity in variances across the samples (as frequently observed in our data) simialrly leads to a loss of statistical power for the test. More powerful tests could be adopted to obtain a further refinement in the assessment of discrepancy, but in this work we focus on providing an overview of where the major discrepancies are found in relation to the generation of surface texture parameters. Noting that discrepancies exist, we then perform further analysis to understand why the parameters are discrepant.

Direct topography comparison provides this deeper course of analysis when there are discrepancies between generated parameters. Top surface measurements were shown to be more repeatable than side surface measurements, with mean CI widths consistently taking higher values in the side surface case (figure 10). The stable ratio of side surface CI width to top surface CI width (excepting the XCT case) implies there may be a correlation between repeatability and some quality of the surface, though further research is required to understand what aspect of the surface repeatability is correlated to, and to solidify the statistical significance of this correlation (if any). Global discrepancy between instrument pairs (table 1) also appears to increase with CI width, with increasing confidence intervals increasing the overlap between CIs. It should be noted that this method does not provide information about the causes of discrepancies, but rather provides information as to the location of discrepancies in the data.

Further understanding of the various instruments' ability to measure these surfaces is presented in the point-by-point CIs (figure 11), which highlight areas on the surface that are difficult for each instrument to measure. Some of these regions are consistent for all instruments, while other regions cause issues for some instruments and not others. These data show that poor repeatability often occurs at the outlines of features,
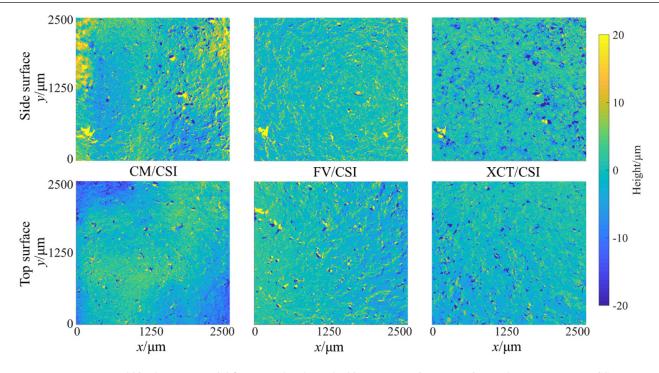
Figure 13. Local bias between spatial frequency band matched instrument pairs, comparing each measurement to CSI.

where high slopes exist, implying a correlation between measurement repeatability and slope characteristics; as could be expected for CM, CSI and FV [14]. This fact is particularly of note in the XCT case, however, where such a correlation would not necessarily be expected, given the volumetric nature of the measurement process. As the XCT data have poor repeatability in similar areas to the other optical data, however, there may also be a correlation between slope and XCT surface measurement repeatability. Further investigation is required to ascertain whether this correlation truly exists, but these results present questions for future study. These plots also reveal other issues present in the measurement process, such as the bow seen in top surface measurement by CM.

Examination of the global discrepancy between surfaces (figure 12) shows regions where measurements are more or less discrepant from one another. Areas that have good or bad repeatability for the whole array of instruments are highlighted, as are areas of good or bad repeatability for individual instruments. For example, there is a region in the bottom left of the side surface measurements in figure 12 where CSI returns different height values compared to the other instruments, though point-by-point CI plots (figure 11) show this area to be very repeatable. Further examination of the raw data (figure 13) shows that this region was an area of non-measured points in each of the CSI measurements, clearly indicating a problematic feature. Most notably, as with metal LPBF surfaces [9], discrepancies between instruments are often similar in size to the features being measured.

Potential improvements to the methods for comparing surfaces presented here should be noted. While measurements were made by skilled operators, further optimisation of instruments is always possible, and further work is required in optimising the systems used during this work for

the measurement of polymer LPBF surfaces. Additionally, as discussed in previous publications [9, 14, 47], while the comparison of replicate measurements of a single measured region represents a deeper method of understanding surfaces than by generation of ISO 4287 or 25178-2 parameters alone, the method has a number of key weaknesses which require development in future studies. Notably, the direct topography comparison method relies on an assumption that the quality alignment between surfaces is negligible, as any alignment error will unnaturally increase any generated CI width. While the iterative closest point algorithm used here is relatively robust, commercial packages that allow researchers and industrialists to do this process reliably are not yet available, and algorithms often fail in ways that are only obvious to a skilled user. Also, the current CI generation model assumes points to be spatially uncorrelated, which is unlikely to be the case. The model, therefore, requires extension to correct for spatial correlation and simultaneous estimation of multiple CIs. Further developments to the CI model are currently in development, and will be the subject of a future publication. Finally, the CI model currently relies on consensus between instruments to provide indications as to the actual topography being measured. In the absence of traceable measurements, this method presents a reasonable solution, but is likely to be insufficient in applications where traceability is a necessity. Without traceability, it is impossible to establish any one technology here as a 'ground truth', so we can only make assumptions about the nature of the surface topography based on consensus between instruments (e.g. if all instruments see a hill in location *x*, it is likely that there is a hill at location *x*). As such, incorporation of traceability into the CI model is a necessary future development, and also the subject of a future publication.

Finally, it should be again noted that in this work we have limited the investigation to showing that differences exist between measurement technologies, as well as how those differences present themselves on the polymer LPBF surface when measured using different technologies. What we have not examined in this investigation is the problem of why these differences exist or how to correct for them; both of these studies represent significant research undertakings and are beyond the scope of this particular publication. The solutions to these issues lie in subsequent research projects and represent interesting undertakings for future work.

5. Conclusion

Measurements of polymer LPBF surfaces have been performed with using contact stylus, CSI, FV, CM and XCT. In all cases, data was acquired with few missing data points and analysis results similar to those acquired using other measurement technologies. Statistical discrepancies between instruments were found between instruments in all cases, but ISO 4287 or 25178-2 parameters generally provided values in similar ballparks for each instrument examined. Examination of local features showed local discrepancies between instruments centred on areas of high slopes. This issue was the case for all optical instruments, including XCT, which acquires fully volumetric data. Discrepancies between instruments were often similar in size to the features on the surface.

This study should be used as a tool to better understand how surface measurement instruments behave when measuring polymer surfaces, and as a demonstration of the technologies capable of measuring such surfaces. Future work is required in optimisation of measurement technologies for polymer LPBF surfaces, and in development of improved methods of comparing surface datasets.

Acknowledgments

ORCID iDs

Adam Thompson ⬤ https://orcid.org/0000-0003-3215-2757
Yann Quinsat ⬤ https://orcid.org/0000-0003-3545-6019
Nicola Senin ⬤ https://orcid.org/0000-0002-9556-0363

References

[1] Gibson I, Rosen D W and Stucker B 2010 *Additive Manufacturing Technologies: 3D Printing, Rapid Prototyping, and Direct Digital Manufacturing* (New York: Springer)

[2] Hon K K B 2007 Digital additive manufacturing: from rapid prototyping to rapid manufacturing *Proc. 35th Int. MATADOR Conf. (London)* pp 337–40

[3] Gao W, Zhang Y, Ramanujan D, Ramani K, Chen Y, Williams C B, Wang C C L, Shin Y C, Zhang S and Zavattieri P D 2015 The status, challenges, and future of additive manufacturing in engineering *Comput. Des.* **69** 65–89

[4] Goodridge R D, Tuck C J and Hague R J M 2012 Laser sintering of polyamides and other polymers *Prog. Mater. Sci.* **57** 229–67

[5] Ngo T D, Kashani A, Imbalzano G, Nguyen K T Q and Hui D 2018 Additive manufacturing (3D printing): a review of materials, methods, applications and challenges *Composites* B **143** 172–96

[6] Rausch A, Küng V, Pobel C, Markl M and Körner C 2017 Predictive simulation of process windows for powder bed fusion additive manufacturing: influence of the powder bulk density *Materials* **10** 1117

[7] King W, Anderson A T, Ferencz R M, Hodge N E, Kamath C and Khairallah S A 2015 Overview of modelling and simulation of metal powder bed fusion process at Lawrence Livermore National Laboratory *Mater. Sci. Technol.* **31** 957–68

[8] Acharya R, Sharon J A and Staroselsky A 2017 Prediction of microstructure in laser powder bed fusion process *Acta Mater.* **124** 360–71

[9] Senin N, Thompson A and Leach R K 2017 Characterisation of the topography of metal additive surface features with different measurement technologies *Meas. Sci. Technol.* **28** 095003

[10] Senin N, Thompson A and Leach R K 2017 Feature-based characterisation of signature topography in laser powder bed fusion of metals *Meas. Sci. Technol.* **29** 045009

[11] Townsend A, Senin N, Blunt L, Leach R K and Taylor J S 2016 Surface texture metrology for metal additive manufacturing: a review *Precis. Eng.* **46** 34–47

[12] Lou S, Jiang X, Sun W, Zeng W, Pagani L and Scott P J 2019 Characterisation methods for powder bed fusion processed surface topography *Precis. Eng.* **57** 1–15

[13] Leach R K, Bourell D, Carmignato S, Donmez A, Senin N and Dewulf W 2019 Geometrical metrology for metal additive manufacturing *Ann. CIRP* **68** 677–700

[14] Thompson A, Senin N, Giusca C and Leach R K 2017 Topography of selectively laser melted surfaces: A comparison of different measurement methods *Ann. CIRP* **66** 543–6

[15] ISO 25178-2 2012 *Geometrical Product Specifications (GPS)—Surface Texture: Areal—Part 2: Terms, Definitions And Surface Texture Parameters* (International Organization for Standardization)

[16] Leach R K 2013 *Characterisation of Areal Surface Texture* ed R K Leach (Berlin: Springer)

[17] ISO 4287 1997 *Geometrical Product Specifications (GPS)— Surface Texture: Profile Method—Terms, Definitions and Surface Texture Parameters* (International Organization for Standardization)

[18] Leach R K 2001 *Good Practice Guide No. 37 The Measurement of Surface Texture Using Stylus Instruments* (London: National Physical Laboratory)

[19] Negi S, Dhiman S and Sharma R K 2014 Investigating the surface roughness of SLS fabricated glass-filled polyamide parts using response surface methodology *Arab. J. Sci. Eng.* **39** 9161–79

[20] Sachdeva A, Singh S and Sharma V S 2013 Investigating surface roughness of parts produced by SLS process *Int. J. Adv. Manuf. Technol.* **64** 1505–16

[21] Vetterli M, Schmid M and Wegener K 2014 Comprehensive investigation of surface characterization methods for laser sintered parts *Proc. Fraunhofer Direct Digital Manufacturing Conf. (Belin, Germany)* pp 221–8

[22] Johnson M K, Cole F, Raj A, Adelson E H, Johnson M K, Cole F, Raj A and Adelson E H 2011 Microgeometry capture using an elastomeric sensor *ACM Trans. Graph.* **30** 1–8

[23] Launhardt M, Wörz A, Loderer A, Laumer T, Drummer D, Hausotte T and Schmidt M 2016 Detecting surface roughness on SLS parts with various measuring techniques *Polym. Test.* **53** 217–26

[24] ISO 25167-607 2019 *Geometrical Product Specifications (GPS)—Surface Texture: Areal—Part 607: Nominal Characteristics of Non-Contact (Confocal Microscopy) Instruments* (International Organization for Standardization)

[25] Artigas R 2011 Imaging confocal microscopy *Optical Measurement of Surface Topography* ed R K Leach (Berlin: Springer) pp 237–86

[26] ISO 2517-606 2015 *Geometrical Product Specifications (GPS)—Surface Texture: Areal—Part 606: Nominal Characteristics of Non-Contact (Focus Variation) Instruments* (International Organization for Standardization)

[27] Helmli F 2011 Focus variation instruments *Optical Measurement of Surface Topography* ed R K Leach (Berlin: Springer) pp 131–66

[28] ISO 25178-604 2013 *Geometrical Product Specifications (GPS)—Surface Texture: Areal—Part 604: Nominal Characteristics of Non-Contact (Coherence Scanning Interferometry) Instruments* (International Organization for Standardization)

[29] Petzing J, Coupland J and Leach R K 2010 *Good Practice Guide No. 116 The Measurement of Rough Surface Topography Using Coherence Scanning Interferometry* (London: National Physical Laboratory)

[30] de Groot P 2015 Principles of interference microscopy for the measurement of surface topography *Adv. Opt. Photonics* **7** 1–65

[31] Disciacca J, Gomez C, Thompson A, Lawes S, Leach R K, De Lega X C and De Groot P 2017 True-color 3D surface metrology for additive manufacturing using interference microscopy *Dimensional Accuracy and Surface Finish in Additive Manufacturing (Leuven, Belgium)* pp 145–8

[32] Thompson A, Maskery I and Leach R K 2018 Internal surface measurement by x-ray computed tomography: an additive manufacturing industrial case study *Dimensional X-ray Computed Tomography (Nottingham, United Kingdom)*

[33] Townsend A, Pagani L, Scott P and Blunt L A 2017 Areal surface texture data extraction from x-ray computed tomography reconstructions of metal additively manufactured parts *Precis. Eng.* **48** 254–64

[34] ISO 25178-3 2012 *Geometrical Product Specifications (GPS)—Surface Texture: Areal—Part 3: Specification Operators* (International Organization for Standardization)

[35] Triantaphyllou A, Giusca C L, Macaulay G D, Roerig F, Hoebel M, Leach R K, Tomita B and Milne K A 2015 Surface texture measurement for additive manufacturing *Surf. Topogr.: Metrol. Prop.* **3** 24002

[36] Digital Surf 2019 Mountains® Surface Imaging & metrology software (https://www.digitalsurf.com/software-solutions/multi-purpose/) (Accessed: 6 January 2020)

[37] Volume Graphics 2019 VGStudio MAX 3.0 (https://www.volumegraphics.com/en/products/vgstudio-max.html) (Accessed: 6 January 2020)

[38] Kiekens K, Welkenhuyzen F, Tan Y, Bleys P, Voet A, Kruth J-P P and Dewulf W 2011 A test object with parallel grooves for calibration and accuracy assessment of industrial computed tomography (CT) metrology *Meas. Sci. Technol.* **22** 115502

[39] Ferrucci M, Haitjema H and Leach R K 2018 Dimensional metrology *Basics of Precision Engineering* ed R K Leach and S Smith (Boca Raton, FL: CRC Press) pp 151–204

[40] MathWorks 2018 Matlab 2018a (https://uk.mathworks.com/products/matlab.html) (Accessed: 6 January 2020)

[41] Thompson A, Senin N, Maskery I, Körner L, Lawes S and Leach R K 2018 Internal surface measurement of metal powder bed fusion parts *Addit. Manuf.* **20** 126–33

[42] Gower J C 1975 Generalized procrustes analysis *Psychometrika* **40** 33–51

[43] Besl P J and McKay N D 1992 A method for registration of 3D-shapes *IEEE Trans. Pattern Anal. Mach. Intel.* **14** 239–56

[44] Minitab 17 2019 Minitab (https://www.minitab.com/en-us/products/minitab/) (Accessed: 6 January 2020)

[45] ISO 4288 1996 *Geometrical Product Specifications (GPS)—Surface Texture: Profile Method—Rules and Procedures for the Assessment of Surface Texture* (International Organization for Standardization)

[46] Leach R K and Haitjema H 2010 Bandwidth characteristics and comparisons of surface texture measuring instruments *Meas. Sci. Technol.* **21** 32001

[47] Thompson A, Senin N, Maskery I and Leach R K 2018 Effects of magnification and sampling resolution in x-ray computed tomography for the measurement of additively manufactured metal *Precis. Eng.* **53** 54–64